Equivalent cellular-based electrical network models for voltage regulation using hybrid conversion technologies at the medium-voltage level

Anna Traupmann[1], Matthias Greiml[1], Thomas Kienberger[1]*

[1]*Montanuniversitaet Leoben, Chair of Energy Network Technology, Franz-Josef-Straße 18, 8700 Leoben, Austria*
**anna.traupmann@unileoben.ac.at*

Keywords: ELECTRICAL NETWORKS, RENEWABLE ENERGY SOURCES, NETWORK REDUCTION, CELLULAR APPROACH, HYBRID FLEXIBILITY OPTIONS

Abstract

Expanding and integrating renewable energy sources (RES) challenges today´s energy systems, especially, electrical grids. Therefore, efficient RES integration methods have to be developed. This work chooses a multi-energy systems (MES) approach using the modelling framework HyFlow, developed at the Chair of Energy Network Technology. For this approach, simplified cellular-based electrical network models are developed using a specific network reduction method that enables these models to be used as an equivalent of the complex original grid since it shows equal electrical behaviour. As an example, this work uses a medium-voltage European test grid with massive volatile RES (wind and photovoltaic) expansion. This will show how this method can stabilize the grid and improve power quality using hybrid flexibility technologies (heat pumps (HP) and Power-to-Gas units (PtG)). Thus, grid expansion measures can be avoided, and self-sufficiency can be increased by this approach.

1 Introduction

Integrating renewable energy sources (RES) into electrical grids requires efficient implementation approaches, since especially volatile and unpredictable RES, such as wind and solar power, will have to increase on a large scale to meet the climate goals. The fluctuations in power generation occurring due to these RES put strain on electrical grids and may cause power quality issues as well as grid congestions. [1-3] Solution approaches for enabling grid-friendly operation and at the same time advancing RES expansion are, for example, multi-energy systems (MES), which relieve electrical grids by shifting surplus electrical energy into another energy carrier network. The MES modelling framework HyFlow [4,5] supports the integration of RES into electrical grids by using a cellular approach for the modelling of different energy carrier networks providing spatial resolution reduction to enable faster calculations and creating coupling points between energy carrier grids. [5] This paper presents a study of a medium-voltage grid, showing how hybrid technologies can be used to enhance power quality issues caused by RES and increase self-sufficiency.

2. Methodology

2.1 Cellular Modelling Approach and Network Reduction

Integrating different energy carrier models into one framework, like HyFlow, requires a modelling approach that is generic and modular in its application. A cellular approach offers this possibility and supports spatial resolution reduction to allow reasonable calculation times of expanded networks with fine temporal resolution. By combining or deleting electrical network elements (nodes and lines) it allows for a grid representation that enables advantages for cross-energy carrier networks. The real network is divided into energy cells representing the lowest system level for which energy balancing using corresponding residual loads $P_{res}(t)$ (by e.g., 15-minute-values) can be achieved. [5-7] The residual load $P_{res}(t)$ is defined as the difference between load $P_{load}(t)$ and generation $P_{gen}(t)$, as shown in Equation (1). [5]

$$P_{res}(t) = P_{load}(t) - P_{gen}(t) \quad (1)$$

A defined set of network nodes is assigned to each cell, depending on geographical aspects. Size, location, and number of assigned nodes of each cell depend on the application purpose. For each cell consumer and generation units are aggregated into a fictitious node in the cell centre to be represented by a small set of parameters. [5-7] Thus, the level of detail of the network model is decreased, however, information influencing the electrical behaviour is lost and has to be compensated using network reduction. The lost information refers to the line losses of the neglected lines within the cells. A specifically developed network reduction method is used to replicate these losses using a compensation module to represent the total line losses of each cell. The module is parameterized using the electrical line parameters (R, L and C) of the neglected lines (Fig. 1). This method allows for the less complex cell model to be used equivalently to the real network and its use in HyFlow. Fig. 1 shows the cellular approach including the network reduction method. [8]

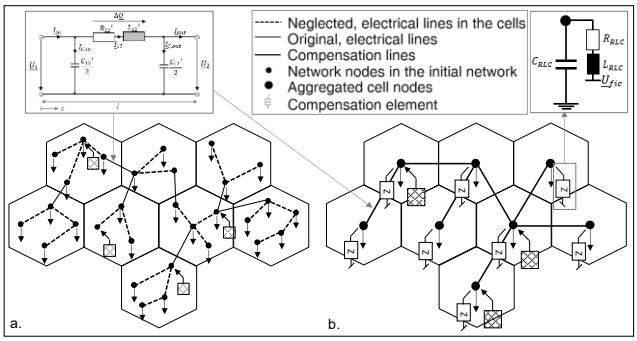

Fig 1: Cellular Modelling Approach with integrated compensation modules using network reduction

2.2 Test Network Description

The used test network represents a 20 kV-medium-voltage public power distribution grid developed from literature data. [9] Fig. 2 shows the original test network including the chosen cell division for the expansion scenario and the corresponding reduced cell model depicted in NEPLAN [10].

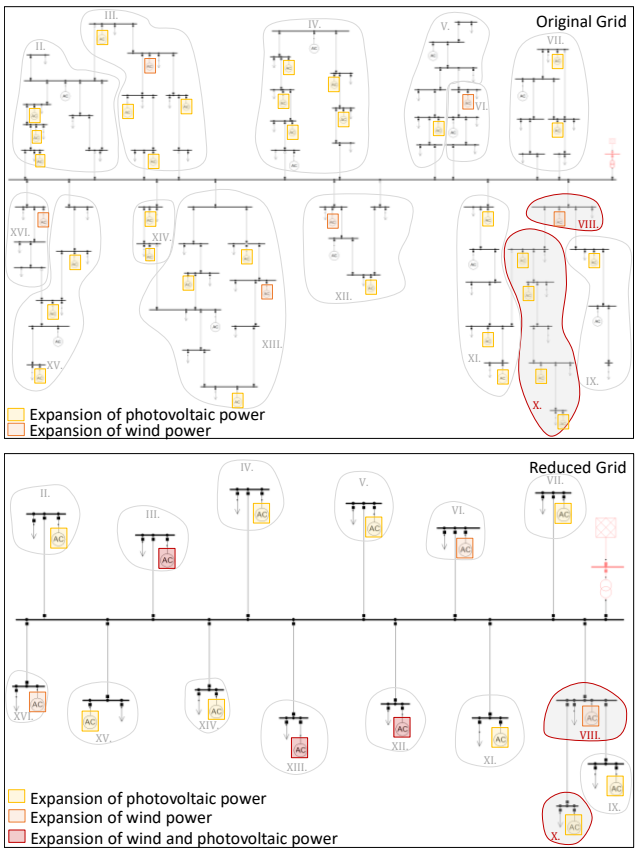

Fig. 2: Original network with cell division and PV/wind expansion and corresponding reduced model

The original network consists of 74 network nodes with 64 consumer units (local substations and commercial consumers represented by standard and synthetic load profiles) and 15 generation units (solar power, biomass plants, geothermal power plants and run-of-river power stations). A closer description of the network and its parameters can be found in [9]. The original test network is reduced to 16 cells (reduction of network size by 78.38 %), thereby, accelerating calculation times by 96.35 %. This work develops an expansion scenario in which the share of photovoltaic (PV) and wind power units is massively increased in the test network compared to its current state described in [9]: Each commercial consumer unit is equipped with a corresponding PV system, additionally, existing wind power plants are expanded and new wind sites are added. For the analysis two cells (Cell VIII and Cell X) are chosen, which are marked in Fig. 2. While the renewable expansion in Cell VIII is an enlargement of the existing wind power plant, PV-system installations are used for the expansion in Cell X.

Due to the volatile renewable expansion a voltage increase is detected for the node in Cell VIII (Fig. 4) and Cell X (Fig. 5). However, to ensure a stable energy supply, the nodal voltages must be within the tolerance range (0.935-1.045 p.u.) of the nominal voltage. If these limits are exceeded, e.g., due to increased renewable generation, overvoltages occur which can damage electrical equipment and cause power quality issues as well as voltage instability.

2.3 Hybrid Flexibility Options

MES offer many advantages such as cascaded energy use and increased energy system efficiency as well as stability by using synergies and coupling different energy carrier networks. [2,3,5] The hybrid flexibility options implemented at the cell nodes, to achieve these advantages, are Power-to-Gas (PtG) units and heat pumps (HP). Therefore, besides PV-units (section 2.2), each commercial consumer is given a heat demand, which is covered by the corresponding HP. PtG units are implemented in cells where only wind power is expanded.

HyFlow uses a rule-based approach for the operation of hybrid flexibility units. This approach distinguishes between cell-serving and system-serving operation. Cell-serving elements aim to minimize the residual load of the corresponding cell, while system-serving elements aim to minimize the residual load of the overall system. HPs follow a cell-serving operation strategy in HyFlow, thus, they operate if there is heat demand or surplus electricity available within that cell. Therefore, to enable maximum stability support by ensuring that the electrical surplus energy of these cells can be converted to heat even if there is no heat demand at that time, a significantly oversized heat storage unit is implemented together with the HP in this work. PtG units, however, are operated in a system-serving strategy. This means that they operate if consumption and generation within the overall system is unbalanced. In this case, to ensure maximum stability support by the PtG units, the produced gas is fed into a connected gas pipeline storing the produced gas unlimitedly. [4]

2.4 KPIs for Energy Balancing in Cellular-Based Networks

In order to evaluate the efficiency of energy use and, thus, energy balancing within each cell, energy indicators are utilized. These energy indicators (energy self-sufficiency

$\mathcal{E}_{ESS}$, power self-sufficiency $\mathcal{E}_{PSS}$ and energy self-consumption ratio $\mathcal{E}_{SCR}$) are explained based on the loads and generations of Cell X. In Fig. 3, $P_{gen}(t)$ represents the power that is provided from local generation in Cell X for the respective time step t. E_{gen} indicates the area under the $P_{gen}(t)$ curve representing the generated energy for the time period. $P_{load}(t)$ from Fig. 3 represents the locally consumed electrical power of Cell X, the area under this curve, therefore, indicates the consumed energy E_{load}. The intersection of E_{gen} and E_{load} represents the self-consumption E_{SC}, meaning the energy that is generated and directly consumed within that cell. The self-consumption is defined according to Equation (2). [11]

$$E_{SC} = \int min\{P_{load}(t), P_{gen}(t)\}\, dt \qquad (2)$$

The degree of energy self-sufficiency $\mathcal{E}_{ESS}$ indicates how much of the locally generated energy E_{gen} can be locally consumed E_{load} (Equation (3)). Since generated energy quantities can be much higher than the consumed energy, $\mathcal{E}_{ESS}$ can show values above 100 %. The degree of power self-sufficiency $\mathcal{E}_{PSS}$ enables an analysis of the share of self-consumption E_{SC} in relation to the local energy consumption E_{load} (Equation (4)). $\mathcal{E}_{PSS}$, therefore, can never be higher than 100 %. Similarly, the energy self-consumption ratio $\mathcal{E}_{SCR}$ allows analysing the share of self-consumption E_{SC} in relation to the locally generated energy E_{gen}, which limits $\mathcal{E}_{SCR}$ to a maximum of 100 % (Equation (5)). [11]

$$\varepsilon_{ESS} = \frac{E_{gen}}{E_{load}} = \frac{\int P_{gen}(t)dt}{\int P_{load}(t)dt} \qquad (3)$$

$$\varepsilon_{PSS} = \frac{E_{SC}}{E_{load}} = \frac{\int min\{P_{load}(t), P_{gen}(t)\}\, dt}{\int P_{load}(t)dt} \qquad (4)$$

$$\varepsilon_{SCR} = \frac{E_{SC}}{E_{gen}} = \frac{\int min\{P_{load}(t), P_{gen}(t)\}\, dt}{\int P_{gen}(t)dt} \qquad (5)$$

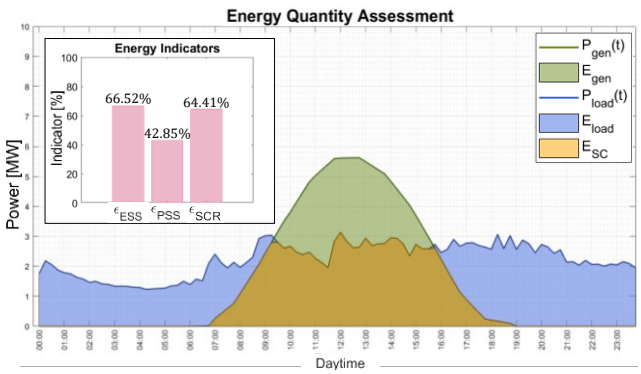

Fig. 3: Energy indicators $\mathcal{E}_{ESS}$, $\mathcal{E}_{PSS}$ and $\mathcal{E}_{SCR}$ on the example of Cell 10

Using storages or hybrid conversion technologies can increase the shares of the energy indicators and, thus, increase energy efficiency.

3 Results

3.1 Expansion Scenario – Base Case

The following figures, Fig. 4 and 5, show the aggregated electrical profiles, energy quantities and the resulting overvoltages for Cell VIII and Cell X discussed in section 2.2.

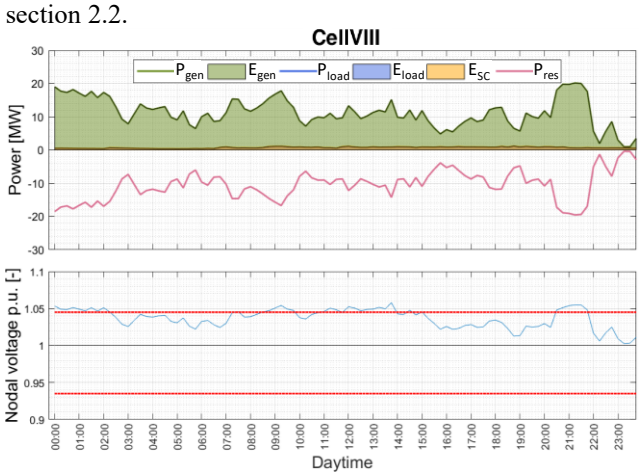

Fig. 4: Electrical profile of Cell VIII and the corresponding nodal voltage time-series before hybrid conversion

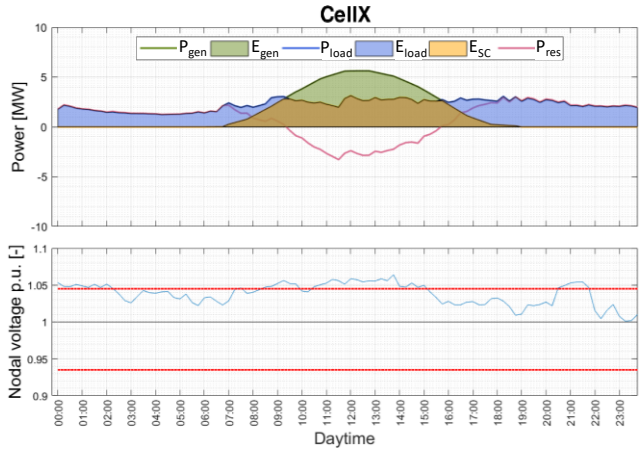

Fig. 5: Electrical profile of Cell X and the corresponding nodal voltage time-series before hybrid conversion

To compensate these voltage limit exceedings due to increased integration of RES into the electrical grid, hybrid elements are implemented at the corresponding cell nodes.

3.2 Prevention of Voltage Limit Violations

The hybrid elements described in section 2.3 implemented within the reduced cellular-based test network model are used in a hybrid load flow calculation in HyFlow. This aims to stabilize nodal voltages within the grid and increase self-sufficiency within single cells as well as the overall system. Thus, Fig. 6 shows the residual load after hybrid conversion $P_{res,hybrid}(t)$ as well as the higher electrical load $P_{load}(t)$ obtained due to the installed PtG unit within Cell VIII. Additionally, it depicts the voltage profile for the corresponding cell node. As can be seen in Fig. 6, the implemented PtG unit enables a smoothed nodal voltage

profile over the examined period of time, showing no overvoltages.

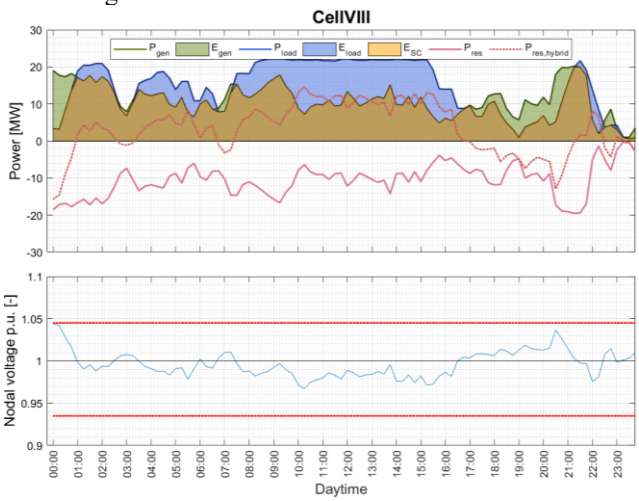

Fig. 6: Electrical profile of Cell VIII and the corresponding nodal voltage time-series after hybrid conversion

Since the services of PtG units cannot be derived directly from a cell-level consideration due to its system-serving operating strategy, Fig. 7 shows how the implemented PtG units within the entire test grid can serve to reduce the residual load at the Slack-node (system boundary). The residual load $P_{res,Slack,hybrid}(t)$ in Fig. 7, however, also includes the influence caused by the implemented HPs within the overall system and is obtained using Equation (6). The load provided by PtG and HP sums up to $P_{conv,hybrid}(t)$.

$$P_{res,Slack,hybrid}(t) = P_{res,Slack}(t) + P_{conv,hybrid} \qquad (6)$$

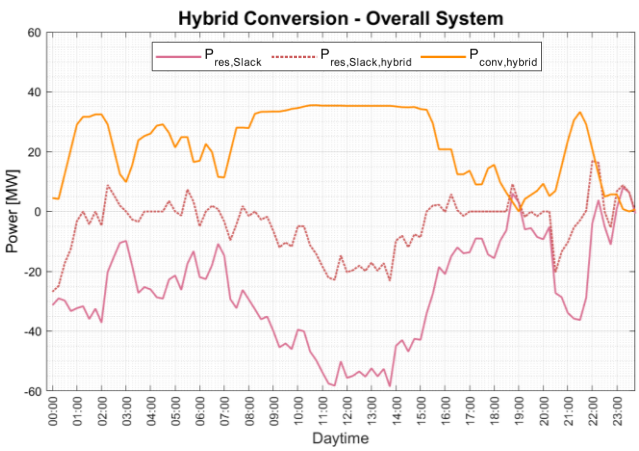

Fig. 7: Hybrid conversion within the overall system at the system boundaries (Slack-node)

The cell-serving operating strategy of the implemented HPs can be observed directly, based on the load and generation situation present within the cell, which is shown on the example of Cell VIII in Fig. 8. Fig. 8, thus, displays the residual load after hybrid conversion $P_{res,hybrid}(t)$ as well as the additional electrical load $P_{load}(t)$ needed to produce the demanded heat by the installed HP of Cell X. Additionally, Fig. 8 depicts the obtained voltage profile of Cell X due to the hybrid conversion. However, since Cell X is the subsequent in the feeder after Cell VIII, its voltage profile is mainly influenced by the smoothed nodal voltage of Cell VIII. Thus, it primarily shows the implications of the PtG unit on the nodal voltage of Cell VIII. Due to the HP and corresponding heat storage, the additional voltage increase caused by high PV-generation around noon can be minimized since most of the negative residual load can be compensated. As a result, violations of voltage limits can successfully be prevented.

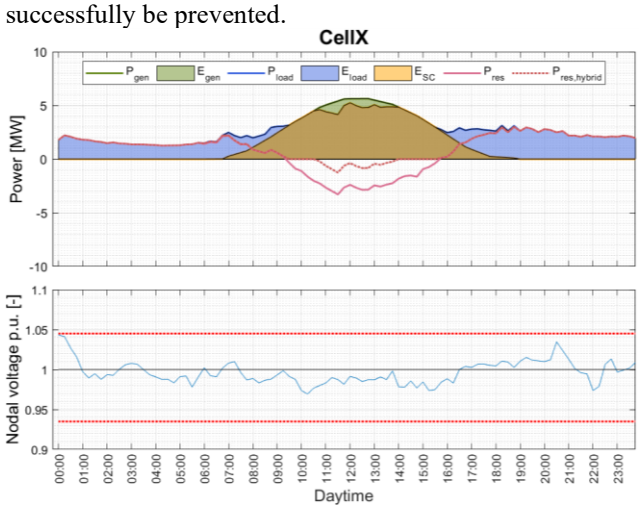

Fig. 8: Electrical profile of Cell X and the corresponding nodal voltage time-series after hybrid conversion

3.3 Energy Balancing

As discussed in section 2.1, a cellular approach can be used to enable efficient energy balancing. Additionally, section 2.3 discussed how MES can increase energy efficiency. Thus, as demonstrated in section 2.4, Fig. 9 shows the energy indicators (energy self-sufficiency $\mathcal{E}_{ESS}$, power self-sufficiency $\mathcal{E}_{PSS}$ and energy self-consumption ratio $\mathcal{E}_{SCR}$) for Cell VIII. Before hybrid conversion, the energy self-sufficiency $\mathcal{E}_{ESS}$ of Cell VIII has a high share of 1536.70 %, which is due to the expansion of wind power within that cell. While the share of power self-sufficiency $\mathcal{E}_{PSS}$ is 100 %, the energy self-consumption ratio $\mathcal{E}_{SCR}$ is very low (6.51 %). This indicates that, although $\mathcal{E}_{ESS}$ and $\mathcal{E}_{PSS}$ are high, the energy use within Cell VIII is not efficient, due to the high amount of surplus renewable energy that cannot be used locally within the cell.

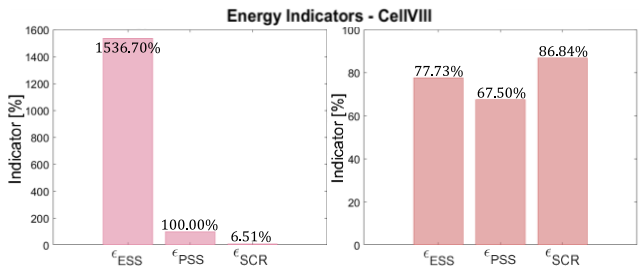

Fig. 9: Energy indicators before (left) and after (right) hybrid conversion within the energy system for Cell VIII

After the hybrid conversion (Fig. 9 (right)), the energy indicators show that the energy use within the cell has increased due to the additional power converted in the PtG unit. This shows that, although the PtG unit is operated using a system-serving strategy minimising the residual load of the overall system and, thus, increasing energy use, it also enhances energy use within single cells.

The energy indicators for Cell X before the hybrid conversion (Fig. 10 (left)) already show efficient energy use with an energy self-sufficiency $\mathcal{E}_{ESS}$ of 66.52 %, a power self-sufficiency $\mathcal{E}_{PSS}$ of 42.85 % and an energy self-consumption ratio $\mathcal{E}_{SCR}$ of 64.41 %. However, as can be seen in Fig. 10 (right), energy use within Cell X can be further enhanced due to the hybrid conversion. The lower values for the energy indicators of Cell X, compared to Cell VIII, are due to the distribution of load and PV-generation within the cell. The electrical energy demand E_{load} is distributed over the entire period of time, while the high PV-generation E_{gen} is only available during daytime. This limits the energy self-consumption E_{SC} and decreases the shares of the energy indicators.

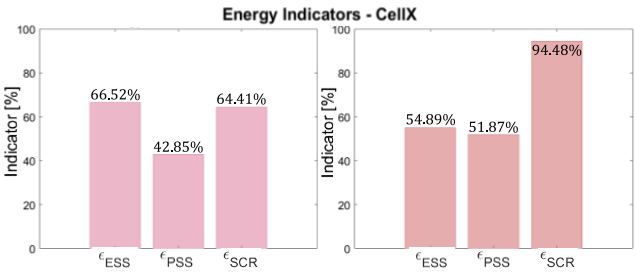

Fig. 10: Energy indicators before (left) and after (right) hybrid conversion within the energy system for Cell X

Although, the share of energy self-sufficiency is lower after hybrid conversion (54.89 %), which is due to the higher energy demand caused by the HP, the energy can be used more efficiently. Especially, the energy self-consumption ratio is very high (94.48 %), indicating that most of the generated energy within Cell X can be used directly within the cell. This reduces the residual load within the cell and, therefore, grid congestions due to energy transportation over the electrical lines between cells.

4 Conclusion

This work presents a study on how innovative approaches (multi-energy systems) and tools (cellular-based electrical networks with network reduction and the hybrid modelling framework HyFlow) can help overcome the challenges of a sustainable energy future. The results obtained from the hybrid load flow calculations show, that hybrid conversion technologies can be used to stabilize voltages and increase power quality. MES can also be used to increase the efficiency of energy use within the energy system. Therefore, the analysis of key energy indicators (energy self-sufficiency $\mathcal{E}_{ESS}$, power self-sufficiency $\mathcal{E}_{PSS}$ and energy self-consumption ratio $\mathcal{E}_{SCR}$) on cell-level shows that by using hybrid conversion technologies, the cellular self-sufficiency can be enhanced. This suggests, that hybrid conversion technologies provide multiple advantages for the future challenges during energy transition.

5 Acknowledgements

This work was carried out as part of the NEFI_Lab project. The NEFI_Lab project is supports with the funds from the Climate and Energy Fund and implemented in the framework of the RTI-initiative “Flagship region Energy”.

6 References

[1] Papadis, E.; Tsatsatsaronis, G.: ‚Challenges in the decarbonization of the energy sector‘, Energy, 2020, 205, pp. 1-15.

[2] Kriechbaum, L.; Scheiber, G.; Kienberger, T.: ‚Grid-based multi-energy systems – modelling, assessment, open source modelling frameworks and challenges ‘, Energy, Sustainability and Society, 2018, 8, (35), pp. 1-19.

[3] Mancarella, P.: ‘MES (multi-energy systems): An overview of concepts and evaluation models’, Energy, 2014, 65, pp. 1-17.

[4] Greiml, M.; Traupmann, A.; Sejkora, C.; Kriechbaum, L.; Böckl, B.; Pichler, P.; Kienberger, T.: ‘Modelling and model assessment of grid-based Multi-Energy Systems’, International Journal of Sustainable Energy Planning & Management, 2020, 29, pp. 7-24.

[5] Böckl, B.; Greiml, M.; Leitner, L.; Pichler, P.; Kriechbaum, L.; Kienberger, T.: ‘HyFlow - A Hybrid Load Flow Modeling Framework to Evaluate the Effects of Energy Storage and Sector Coupling on the Electrical Load Flows’, energies, 2019, 12, p.25.

[6] Vopava, J.; Koczwara, C.; Traupmann, A.; Kienberger, T.: ‚Investigating the impact of e-mobility on the electrical power grid using a simplified grid modeling approach ‘, energies, 2020, 39, p.25.

[7] 15. Vopava, J.; Böckl, B.; Kriechbaum, L.; Keinberger, T.: ‚Anwendung zellularer Ansätze bei der Gestaltung zukünftiger Energieverbundsysteme‘, *e&i* Elektrotechnik & Informationstechnik, 2017, 134, (3), pp. 238-245.

[8] Traupmann, A.; Kienberger, T.: ‘Novel Network Reduction Method for Cellular-Based Networks with High Modelling Accuracy for Multi-Energy System Approaches’ (under submission), 2021.

[9] Traupmann, A.; Kienberger, T.: ‚Test Grids for the Integration of RES – A Contribution for the European Context‘, energies, 2020, 13, p.29.

[10] NEPLAN-Smarter Tools. https://www.neplan.ch/ (accessed on 18th Febuary 2021).

[11] Böckl, B.; Kienberger, T.: ‘Nutzergruppenabhängiger Photovoltaik-Heimspeicherbedarf‘. 15th Symposium Energieinnovation, Graz, February 2018, pp. 6.